# Quantum computing for classical problems: variational quantum eigensolver for activated processes

New Journal of Physics
The open access journal at the forefront of physics

Deutsche Physikalische Gesellschaft DPG
IOP Institute of Physics

Published in partnership with: Deutsche Physikalische Gesellschaft and the Institute of Physics

OPEN ACCESS

RECEIVED
7 September 2021

REVISED
19 November 2021

ACCEPTED FOR PUBLICATION
3 December 2021

PUBLISHED
24 December 2021



PAPER

# Quantum computing for classical problems: variational quantum eigensolver for activated processes

**Pierpaolo Pravatto[1], Davide Castaldo[1], Federico Gallina[1], Barbara Fresch[1,2], Stefano Corni[1,2,3] and Giorgio J Moro[1,2,*]**

[1] Università degli studi di Padova, Dipartimento di Scienze Chimiche, Via Marzolo 1—35131 Padova, Italy
[2] Padua Quantum Technologies Research Center, Università di Padova, Italy
[3] Istituto Nanoscienze—CNR, via Campi 213/A, 41125 Modena, Italy
[*] Author to whom any correspondence should be addressed.

**E-mail:** giorgio.moro@unipd.it

**Keywords:** quantum algorithms, variational quantum eigensolver, Fokker–Planck–Smoluchowski equation, rate constant of activated processes

## Abstract

The theory of stochastic processes impacts both physical and social sciences. At the molecular scale, stochastic dynamics is ubiquitous because of thermal fluctuations. The Fokker–Plank–Smoluchowski equation models the time evolution of the probability density of selected degrees of freedom in the diffusive regime and it is, therefore, a workhorse of physical chemistry. In this paper we report on the development and implementation of a variational quantum eigensolver to solve the Fokker–Planck–Smoluchowski eigenvalue problem. We show that such an algorithm, typically adopted to address quantum chemistry problems, can be effectively applied to classical systems, paving the way to new applications of quantum computers. We compute the conformational transition rate in a linear chain of rotors with nearest-neighbour interactions. We provide a method to encode the probability distribution for a given conformation of the chain on a quantum computer and assess its scalability in terms of operations. A performance analysis on noisy quantum emulators and quantum devices (IBMQ Santiago) is provided for a small chain which shows results in good agreement with the classical benchmark without any further addition of error mitigation techniques.

## 1. Introduction

Since the dawn of quantum mechanics, the study of quantum phenomena has been a key focus of the scientific community. For many years quantum systems have been investigated with the sole purpose of deepening our understanding of their microscopic behaviour. In recent years, however, scientific and technological advancement opened the way to the direct manipulation and control of quantum systems with the aim of solving practical problems. This paradigm shift, sometimes referred to as the second quantum revolution [1], has changed the way we look at the quantum world from an object of study to a powerful new tool. Quantum computation is surely one of the key examples of these new quantum technologies and unearthing computational tasks for which the use of quantum resources can offer a significant increase in efficiency compared to the best classical algorithmic counterpart is one of the key challenges of the field. Much effort in the scientific community has been devoted to this alternative computing paradigm, leading to the development of several algorithms that have demonstrated its disruptive potential [2]. In particular, near-term applications include the quantum simulation of physical and chemical systems [3]. In the present era of noisy intermediate-scale quantum devices (NISQ) [4], hybrid quantum algorithms are a valuable tool for boosting classical computing power using small quantum processors. In this framework, some of the best performing algorithms are the so-called variational hybrid algorithms (VHA). There, the quantum device is in charge of preparing a parameterized trial state and

calculating a cost function that is minimized by an external classical optimization routine [4]. This method requires the quantum device to run reasonably short-depth circuits that cope with the limited coherence time and high error rate of modern NISQ devices [5].

The literature on VHA is constantly growing both in terms of different algorithmic implementations and applications. These range from the electronic structure of small molecules [6, 7] to molecular vibrations [8], and from condensed matter to high-energy physics [9, 10]. In contrast, less attention has been dedicated to the simulation of stochastic systems, i.e. systems characterized by variables with a random character, and thus by classical probability distributions. We believe that combining standard methods of stochastic calculus and the potential of quantum computers can lead to the development of new quantum tools in the simulation of complex system. This can pave the way to important advances in chemistry, biochemistry and all the other fields in which the stochastic analysis plays a relevant role, such as quantitative finance, epidemiology, and computational fluid dynamics [11–13]. Here we propose a new VHA to solve the Fokker–Planck–Smoluchowski (FPS) eigenvalue problem based on the existing isomorphism between the FPS operator and the quantum Hamiltonian [14, 15]. As an example, in this paper, we will focus on the approximation of the kinetic rate constant for the conformational transition in linear chain molecules, that is connected with the first non-vanishing eigenvalue of the FPS operator. Despite its simplicity, this model has been used as a theoretical starting point for the conformational analysis in polymers [16–18], the study of which has profound implications in many different fields [19].

The present contribution is organized as follows: section 2 outlines the theoretical framework of our approach. Firstly, we give a general overview of how the FPS eigenvalue problem can be treated on a quantum computer. Then, we formalize the stochastic description of the conformational dynamics of a chain of rotors characterized by a bistable intramolecular potential energy surface.

This system, which is the case-study of the present work, models the molecular dynamics of simple polymers. An important aspect of the Fokker–Planck dynamics in bistable systems is that the first excited state can become almost degenerate with the ground state especially for large activation barriers. The corresponding small, but non-zero, eigenvalue determines the rate of passage of particles from one potential well to the other, defining a theoretical framework for a microscopic derivation of the rate coefficients of elementary two-state reactions, as initiated by Kramers [20, 21]. Although the first non-zero eigenvalue assumes a central relevance in the study of kinetic processes, an accurate calculation is computationally challenging especially for large systems characterized by many coupled coordinates. In this context, the application of new quantum computational tools can be convenient to possibly tackle previously inaccessible stochastic problems.

We propose to harness the exponential storage capacity of a quantum computer to handle this problem and we detail the implementation of the stochastic problem on a quantum architecture in Section 3. The eigenvalue problem associated to the Fokker–Planck operator is encoded in the quantum register with a simple binary mapping of the basis set to the computational basis. By exploiting the symmetry of the FPS operator, we discuss a VQE-like algorithm to obtain the first non-zero eigenvalue of the stochastic operator, corresponding to the kinetic rate of the isomerization reaction mentioned above.

Section 4 presents the results obtained from the simulation of small chains characterized by different activation barriers. We discuss aspects which play a critical role in the performance of the algorithm, such as the choice of the variational ansatz, the size of the basis set which is reflected in the number of qubits to be used and the effect of the noise on the accuracy of the result. In the concluding section, we critically discuss the potential quantum advantage of the proposed algorithm. The key advantage stems from the linear scaling in terms of memory resources. Indeed, the binary mapping implies a linear relation between the number of rotors in the polymeric chain and the number of qubits used in the implementation. This translates into an exponential gain with respect to the resources of a classical memory, which grow linearly with the dimension of the vector space representing the state of the system, and exponentially with the number of rotors. On the other hand, the present implementation suffers from an exponential scaling in the number of expectation values that have to be measured to solve the problem. This leads to a *de-facto* lack of algorithmic advantage that, as will be discussed, shows an exponential scaling even when proper grouping techniques to reduce the number of measurements are invoked. These issues, together with a limited accuracy in the results for low barriers, represent the main challenges posed by this new approach to the stochastic problem. Starting from these considerations, we therefore point out the future developments that are needed to bring the stochastic molecular dynamics among the applications that will take great advantage of the advent of quantum computers.

## 2. Theory

The stochastic description of molecular systems is a broad research field that embraces a wide range of theoretical tools to allow the interpretation of the fluctuating dynamics of microscopic systems in a plethora of physical conditions [22]. Here, we will focus our attention on the simple case of a stationary and Markovian diffusive process. This kind of behavior is typical of the so-called over-damped regime [23], in which a time-scale separation is observed between the configurational variables' dynamics and the evolution of their conjugated momenta, due to fact that the former is much slower than the latter. By looking at the system within a time-scale comparable with the fluctuations of the configurational variables $\mathbf{q}(t)$, the momentum variables rapidly loose correlation, so that one can assume they are relaxed in the equilibrium distribution.

In order to describe the time evolution of the probability distribution $\rho(\mathbf{q}, t)$, that depends on some configurational variables $\mathbf{q}$, the Fokker–Planck–Smoluchowski (FPS) equation can be invoked [23]:

$$\frac{\partial \rho(\mathbf{q}, t)}{\partial t} := -\hat{\Gamma}\rho(\mathbf{q}, t), \tag{1}$$

where the FPS operator $\hat{\Gamma}$ is defined as follows:

$$\hat{\Gamma} = -\frac{\partial}{\partial \mathbf{q}}^{T} \mathbf{D}(\mathbf{q})\rho_{\mathrm{eq}}(\mathbf{q})\frac{\partial}{\partial \mathbf{q}}\rho_{\mathrm{eq}}(\mathbf{q})^{-1}. \tag{2}$$

Here $\mathbf{D}(\mathbf{q})$ is the diffusion tensor [23] and $\rho_{\mathrm{eq}}(\mathbf{q})$ represents the Boltzmann equilibrium probability distribution:

$$\rho_{\mathrm{eq}}(\mathbf{q}) \propto \mathrm{e}^{-\beta U(\mathbf{q})}, \tag{3}$$

where $U(\mathbf{q})$ is the mean-field potential and $\beta = (k_{\mathrm{B}}T)^{-1}$.

The FPS operator is real and positive semi-definite such that each eigenvalue $\lambda_k$ obeys to the constraint $\lambda_k \geqslant 0\ \forall k$. From now on we will consider the eigenvalues $\lambda_k$ sorted in ascending order such that $\lambda_k \leqslant \lambda_{k+1}$ and we will indicate with $\psi_k(\mathbf{q})$ the corresponding eigenfunctions.

The first eigenfunction $\psi_0(\mathbf{q})$, corresponding to the null eigenvalue $\lambda_0 = 0$, is provided by the equilibrium distribution $\rho_{\mathrm{eq}}(\mathbf{q})$. In fact, if the time evolution of a generic non-equilibrium distribution $\rho(\mathbf{q}, t) = \sum_k c_k(t)\psi_k(\mathbf{q})$ is considered, the following relation holds:

$$\rho(\mathbf{q}, t+\tau) = \mathrm{e}^{-\hat{\Gamma}\tau}\rho(\mathbf{q}, t) = \sum_k \mathrm{e}^{-\lambda_k\tau}c_k(t)\psi_k(\mathbf{q}). \tag{4}$$

From this equation one can easily see that, since all the non-zero eigenvalues play the role of exponential decay rates, a generic probability distribution must relax to $\psi_0(\mathbf{q})$, which must therefore be the equilibrium state.

The aim of this work is to investigate a possible strategy to solve, with the support of a quantum computer, the eigenvalue problem associated with the FPS operator in equation (2). This cannot be done directly since the FPS operator is not Hermitian and, as such, cannot be converted into a qubit Hamiltonian to be used in the variational procedure. Fortunately, this issue has a simple work-around that involves the introduction of a symmetrized, self-adjoint operator $\hat{\tilde{\Gamma}}$:

$$\hat{\tilde{\Gamma}} := \rho_{\mathrm{eq}}(\mathbf{q})^{-\frac{1}{2}}\hat{\Gamma}\rho_{\mathrm{eq}}(\mathbf{q})^{\frac{1}{2}} \tag{5}$$

which leads to a 'Schrödinger-like' representation of the FPS operator [15] with $\hat{\tilde{\Gamma}}$ in place of the Hamiltonian operator.

This new symmetrized operator has the same eigenvalues $\lambda_k$ of the original FPS operator, while its eigenfunctions $\tilde{\psi}_k(\mathbf{q})$ are obtained from the eigenfunctions $\psi_k(\mathbf{q})$ of $\hat{\Gamma}$ according to the relation:

$$\tilde{\psi}_k(\mathbf{q}) = \rho_{\mathrm{eq}}(\mathbf{q})^{-\frac{1}{2}}\psi_k(\mathbf{q}). \tag{6}$$

For more details about the symmetrized FPS operator we refer to [23, 24].

Here, inspired by the variational quantum eigensolver (VQE) [25], we propose an hybrid algorithm to compute the first non-vanishing eigenvalue (i.e. $\lambda_1$) of $\hat{\tilde{\Gamma}}$. The procedure exploits the quantum computer to prepare, by means of a parametrized circuit, a trial wave-function to approximate the state of the target eigenfunction $\tilde{\psi}_1(\mathbf{q})$. Subsequently an external classical optimization routine updates the parameters of the variational circuit on the basis of the measured expectation value $\langle\hat{\tilde{\Gamma}}\rangle$. The procedure is iterated until

convergence. In order to measure $\langle\hat{\tilde{\Gamma}}\rangle$, the symmetrized FPS operator will be represented as a linear combination of Pauli strings

$$\begin{aligned}\hat{\Gamma}_{\mathrm{QC}} &= \sum_j \gamma_j \hat{P}_j \\ \langle\hat{\tilde{\Gamma}}\rangle \equiv \langle\hat{\Gamma}_{\mathrm{QC}}\rangle &= \sum_j \gamma_j \langle\hat{P}_j\rangle,\end{aligned} \tag{7}$$

where the explicit formulation for the weights $\gamma_j$ and the Pauli strings $\hat{P}_j \in \{\sigma_x, \sigma_y, \sigma_z, \mathbb{I}\}^{\otimes N}$ depends upon the adopted mapping (see section 3).

Notably, the direct application of the VQE procedure to the FPS eigenvalue problem would lead, as already mentioned, to the trivial solution $\lambda_0 = 0$. In section 2.1 the solution of this issue will be discussed and we will report on the implementation of a particular problem in which the symmetry of the system allows to easily target the desired eigenvalue. In the same section, a general discussion is presented for the case of systems in which such symmetry relation is lacking. As will be presented, the particular nature of the stochastic problem, in which the equilibrium state is known, will allow us to project out of the problem the trivial solution. This feature sets the stochastic problem apart from the electronic one allowing the computation of excited states without the need of invoking more advanced computational techniques usually employed in the context of computing the excited states of a molecular Hamiltonian [26–28].

In the following section we will present a linear chain molecule as a model system to implement the procedure sketched above. We will focus on the calculation of the first excited state that, as will be discussed, assumes a central relevance in the study of kinetic processes.

### 2.1. Stochastic dynamics and conformational transition rate

The FPS equation describes the time evolution of the probability distribution over all the configurational domain, allowing for a continuous description of the system dynamics. This degree of detail is surely very informative, but is also not always the best way of describing a reactive process. Often, either for simplicity or due to the lack of information about the initial distribution, less detailed descriptions are adopted, in which, rather than describing the molecular configurations, one usually thinks to the process as the interconversion between reactant and product structures [15]. In doing so we implicitly moved our description from a continuous FPS problem to a discrete master equation with rates identifying the kinetic constants for the interconversions between different states.

In this paper, we will consider a symmetrical double minimum system in which two stable molecular configurations are kept apart by a potential barrier. This is the prototypical example of a simple isomerization process in which the kinetic constants $k$ of the direct and reverse processes are the same. When a master equation description is adopted, it is trivial to show how the population relaxation rate toward equilibrium is described by the exponential decay $\exp(-2kt)$. If the barrier is large enough, the FPS operator eigenvalue spectrum shows a large gap between the first non-zero eigenvalue $\lambda_1$ and the higher ones. In this picture, the states corresponding to $\lambda_n \gg \lambda_1$ have the character of fast (intra-minimum) relaxing modes, while the longer-lived state, corresponding to $\lambda_1$, represents the kinetic relaxation mode connected with the population transfer between sites (figure 1). The exponential form dictating the relaxation dynamic can be obtained from equation (4) as $\exp(-\lambda_1 t)$ from which the simple relation, $\lambda_1 = 2k$, can be established between the kinetic constant $k$ and the first non-vanishing FPS operator eigenvalue $\lambda_1$.

### 2.2. The rotor chain as a model for molecular conformational dynamics

Now that the theoretical framework has been outlined, let us introduce a model system to be used as a test subject. We consider a chain of $N+1$ rotors that are free to rotate around a common axis, see figure 2. Let $\varphi_k$ (for $k = 0, 1, \ldots, N$) be the angular coordinate representing the orientation of the $k$th rotor with respect to a laboratory axis orthogonal to the chain axis. We define $\theta_k := \varphi_k - \varphi_{k-1}$ as the relative orientation angles, hereafter called as dihedral angles, between the $k$th rotor and the previous one in the chain.

Let us assume that the rotors interact on the basis of a nearest-neighbour periodic potential $U_k(\theta_k) = U_k(\theta_k + 2\pi)$, depending on the corresponding dihedral angle $\theta_k$. The overall mean-field potential of the chain can be specified as:

$$U(\boldsymbol{\theta}) := \sum_{k=1}^{N} U_k(\theta_k) \tag{8}$$

in which $\boldsymbol{\theta} = (\theta_1, \ldots, \theta_N) \in \mathbb{R}^N$ represents the vector encoding the internal configuration of the chain.

In order to have a clear picture of the kinetic process, we consider a chain in which $N-1$ mono-stable dihedrals are coupled to a single bi-stable potential. In what follows, the mono-stable potential will be

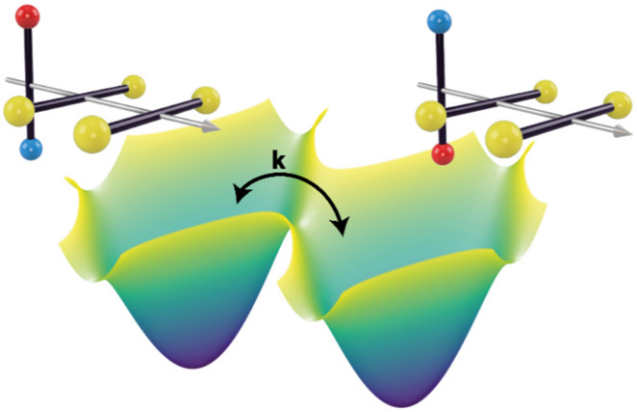


**Figure 1.** Pictorial representation of the isomerization process in the chain of three rotors. The potential energy surface corresponds to the two different configurations of the chain molecule, the kinetic rate constant for the process is determined by the first non-zero eigenvalue of the Fokker–Planck–Smoluchowski operator.

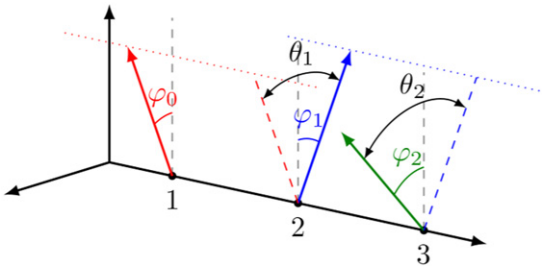


**Figure 2.** Schematic representation of a chain of three rotors reporting the definition of the set of $\varphi_k$ orientations and of the corresponding set of dihedral angles $\theta_k$.

specified as:

$$U_k(\theta_k) := \frac{\Delta_{\mathrm{nr}}}{2}\left[1 - \cos(\theta_k)\right] \tag{9}$$

while the bi-stable one by the form:

$$U_k(\theta_k) := \frac{\Delta_{\mathrm{r}}}{2}\left[\cos(2\theta_k) + 1\right], \tag{10}$$

where we have adopted the symbols $\Delta_{\mathrm{r}}$ and $\Delta_{\mathrm{nr}}$ to indicate the barrier height encountered when moving, respectively, along the *reactive* and *non-reactive* dihedral coordinates.

Furthermore, we assume the absence of hydrodynamic interactions [19] among the rotors which, therefore, are considered as characterized by independent and constant diffusion coefficients ($D_k$ for $k = 0, 1, \ldots, N$). Under these assumptions the FPS operator for the process can be written as:

$$\hat{\tilde{\Gamma}} = -\sum_{k=0}^{N} D_k \rho_{\mathrm{eq}}^{-\frac{1}{2}}(\boldsymbol{\varphi}) \frac{\partial}{\partial \varphi_k} \rho_{\mathrm{eq}}(\boldsymbol{\varphi}) \frac{\partial}{\partial \varphi_k} \rho_{\mathrm{eq}}^{-\frac{1}{2}}(\boldsymbol{\varphi}) \tag{11}$$

in which $\boldsymbol{\varphi} = (\varphi_0, \ldots, \varphi_N) \in \mathbb{R}^{N+1}$ represents the vector encoding the orientation of each rotor.

The FPS operator defined in equation (11) contains a degenerate degree of freedom. Because of the pairwise decomposition of the mean field potential (see equation (8)), any homogeneous rotation of the rotors brings the system into an equivalent conformational state. Such a degeneracy can be exploited by introducing a coordinate representation based on the dihedral angles $\boldsymbol{\theta}$ and the overall chain orientation $\Phi$ defined as:

$$\Phi := \frac{\sum_{k=0}^{N} \frac{\varphi_k}{D_k}}{\sum_{k=0}^{N} \frac{1}{D_k}}. \tag{12}$$

If the coordinate transformation $\boldsymbol{\varphi} \rightarrow [\Phi, \boldsymbol{\theta}]$ is applied, the FPS operator can be decomposed as the sum of a global orientation operator $\hat{\tilde{\Gamma}}_\Phi$, $N$ single-dihedral terms $\hat{\tilde{\Gamma}}_k$ and $N-1$ two-dihedral interaction terms $\hat{\tilde{\Gamma}}_{k,k+1}$:

$$\hat{\tilde{\Gamma}} \rightarrow \hat{\tilde{\Gamma}}_\Phi + \sum_{k=1}^{N} \hat{\tilde{\Gamma}}_k + \sum_{k=1}^{N-1} \hat{\tilde{\Gamma}}_{k,k+1} \tag{13}$$

with these operators specified as:

$$\hat{\tilde{\Gamma}}_\Phi = -\frac{1}{\sum_{k=0}^{N} D_k^{-1}} \frac{\partial^2}{\partial \Phi^2} \tag{14}$$

$$\hat{\tilde{\Gamma}}_k = -\left(D_k + D_{k-1}\right)\left[\frac{\partial^2}{\partial \theta_k^2} + \frac{U_k''(\theta_k)}{2} - \frac{U_k'(\theta_k)^2}{4}\right] \tag{15}$$

$$\hat{\tilde{\Gamma}}_{k,k+1} = 2D_k\left[\frac{\partial}{\partial \theta_k}\frac{\partial}{\partial \theta_{k+1}} - \frac{1}{4}U_k'(\theta_k)U_{k+1}'(\theta_{k+1})\right]. \tag{16}$$

In order to study the conformational dynamics, the term $\hat{\tilde{\Gamma}}_\Phi$, depending on the global orientation angle $\Phi$, can be neglected since it does not affect the internal degrees of freedom.

At this point, in order to solve the eigenvalue problem associated with the FPS operator and to obtain the integrals required for the VQE algorithm, a convenient basis set should be selected. For the purpose of this paper a set of composite basis functions $\{\phi_{\mathbf{n}}(\boldsymbol{\theta})\}$ has been constructed according to:

$$\phi_{\mathbf{n}}(\boldsymbol{\theta}) = \prod_{k=1}^{N} \Xi_{n_k}(\theta_k), \tag{17}$$

where $\Xi_{n_k}(\theta_k)$ are the eigenfunctions of the single dihedral operator $\hat{\tilde{\Gamma}}_k$ and $\mathbf{n} = (n_1, \ldots, n_N)$ represents a vector containing the order of the eigenfunctions for each dihedral angle. All the isolated dihedral eigenfunctions $\Xi_{n_k}(\theta_k)$ have been obtained by expanding the proper FPS operator over a Fourier basis set.

Given the parameterized forms of equations (9) and (10) for the contributions to the mean field potential, one can demonstrate quite easily that the FPS operator $\hat{\tilde{\Gamma}}$ is invariant with respect to the change of sign of all the dihedral angles. In mathematical terms this condition implies the commutation relation $\left[\hat{\Gamma}, \hat{S}\right] = 0$, where $\hat{S}$ is the symmetry operator for the change of sign of the dihedral angles. In essence, the FPS operator acts on a symmetry parted Hilbert space $\mathcal{H} = \mathcal{H}_+ \oplus \mathcal{H}_-$ and its action does not mix functions belonging to the even $\mathcal{H}_+$ and the odd $\mathcal{H}_-$ sub-spaces. Thus, the variational theorem applies to the lowest eigenvalue of both sub-spaces. Therefore, the first eigenstate $\tilde{\psi}_0(\mathbf{q}) = \rho_{\mathrm{eq}}(\mathbf{q})^{-\frac{1}{2}}$ and the second eigenstate $\tilde{\psi}_1$, that is associated with the aforementioned kinetic mode, can be obtained from variational procedures on the even and odd sub-spaces, respectively. In our framework, the application of a VQE procedure to get $\lambda_1$ requires the representation of FPS operator only on the basis of the odd basis functions.

Given $p_{n_k} \in (-1, 1)$ as the parity index of each dihedral eigenfuntion $\Xi_{n_k}(\theta_k)$, the condition:

$$\prod_{k=1}^{N} p_{n_k} = -1 \quad \forall\ \mathbf{n} | \phi_{\mathbf{n}}(\boldsymbol{\theta}) \in \mathcal{H}_- \tag{18}$$

must be verified in order to consider only functions belonging to the odd $\mathcal{H}_-$ sub-space. The results of the classical computations of the stochastic problem will be discussed, together with the ones obtained using the VQE procedure, in section 4.

Of course the previous procedure can be employed only to internal potentials which are symmetric with respect to the change of sign of dihedral angles. When dealing with an internal potential due to nearest-neighbour interactions without such a symmetry, one should take into account that the stationary solution of the FPS operator $\hat{\tilde{\Gamma}}$ is given as the product of the stationary solutions of single dihedral operators $\hat{\tilde{\Gamma}}_k$, that is the basis function $\phi_{\mathbf{n}^0}(\theta)$ with an index vector $\mathbf{n}^0 = (0, 0, 0, \ldots)$ with vanishing components. Thus, the variational procedure for the calculation of the first non-vanishing eigenvalue $\lambda_1$ can be applied to the Hilbert subspace defined by the orthogonality with respect to the stationary solution, that is the subspace spanned by basis functions $\phi_{\mathbf{n}}(\theta)$ with $\mathbf{n} \neq \mathbf{n}^0$. The computational cost of this generalization is that of nearly doubling the dimension of the required matrix representation, corresponding to an increase by one qubit of the quantum computer. In all generality the variational procedure can always be applied to the calculation of the first non-vanishing eigenvalue of the FPS operator

$\hat{\tilde{\Gamma}}$ by representing it onto the subspace orthogonal to the stationary solution which is known in advance as the equilibrium distribution of the stochastic model.

## 3. Implementation

The first step in the implementation is represented by the translation of the target $\tilde{\psi}_1(\mathbf{q})$ eigenfunction from a linear combination of $N$-dihedral states (equation (17)) to a linear combination of bit-string states in the quantum computer. Such a procedure will provide also an expression for the symmetrized FPS operator as a combination of Pauli strings. In this paper, we opted for a binary mapping in which a progressive numerical label $j$ is assigned to every basis function $\phi_{\mathbf{n}}(\boldsymbol{\theta})$. Each label is then directly mapped through its binary representation bin($j$) in a state $|j\rangle \equiv |\text{bin}(j)\rangle$ of the quantum register. Given a set of $J$ basis functions a total of $Q = \lceil \log_2(J) \rceil$ qubits is required.

We start the mapping process by considering the FPS operator representation in the previously introduced symmetry-adapted basis:

$$\hat{\tilde{\Gamma}} = \sum_{r,c} \gamma_{r,c} |r\rangle\langle c| \quad \text{with} \quad \gamma_{r,c} = \langle r|\hat{\tilde{\Gamma}}|c\rangle. \tag{19}$$

Let us indicate with $\delta_q(j)$ the $q$th digit of the binary representation of $j$ such that $|j\rangle \equiv |\delta_1(j), \ldots, \delta_Q(j)\rangle$, we can rephrase the operator representation, equation (19), in a qubit-wise form:

$$\hat{\tilde{\Gamma}} = \sum_{r,c} \gamma_{r,c} \bigotimes_{q=1}^{Q} |\delta_q(r)\rangle\langle\delta_q(c)|. \tag{20}$$

Expressing each single qubit outer product as combination of Pauli matrices, we obtain the following linear combination of Pauli strings like in equation (7):

$$\hat{\tilde{\Gamma}} = \sum_{r,c} \gamma_{r,c} \bigotimes_{q=1}^{Q} \left\{ \frac{1 - |\delta_q(r) - \delta_q(c)|}{2} \left[1_q + (-1)^{\delta_q(r)} \boldsymbol{\sigma}_q^z\right] + \frac{|\delta_q(r) - \delta_q(c)|}{2} \left[\boldsymbol{\sigma}_q^x + (-1)^{\delta_q(r)} i\boldsymbol{\sigma}_q^y\right] \right\}. \tag{21}$$

As can be seen, each matrix element of the FPS operator is translated into a set of $2^Q$ strings, composed by $Q$ Pauli matrices. Each set of strings is specific for the given binary bit-string representation of all the possible $r$ and $c$ states.

Now, we discuss the potential quantum advantage of this approach. Considering that the number of basis states $J$ to encode shows a roughly exponential increase with the system size (e.g. with the length of the rotor chain), this mapping allows to overcome the exponential growth of a classical storage space by requiring a number of qubits which scales linearly with the system size. To be more precise, let us indicate with $m$ a positive integer related to the number of single-dihedral basis states used to set up the product states in equation (17) and let $N$ be the number of dihedral angles in the chain. From these assumptions, we can estimate the order of $J$ to be $J \sim \mathcal{O}(m^N)$ and, consequently, only $\mathcal{O}(N \log_2(m))$ qubits are needed to represent the system on the quantum register. In order to fully characterize the efficiency associated with the procedure, a more in depth analysis of the mapping is required. To do so, the measurement process has to be taken into account. As mentioned in section 2, the expectation value measurement is related, according to equation (7), to the expectation values of the Pauli strings which, in turn, are affected by both the structure of the operator and the mapping. Since we have already discussed the features of the mapping, now we should turn our attention to the estimation of the non-vanishing elements of the FPS operator.

Due to the nearest-neighbour nature of the interaction the $\hat{\tilde{\Gamma}}$ operator is sparse. Indeed, it has a block-structure where only states differing for single-dihedral function of adjacent rotors are connected. Nevertheless, even with this great reduction, the number of Pauli strings to be measured is exponential: the number of elements connecting states that differ for two single-dihedral functions is $\mathcal{O}(m^2JN)$, to which we add the $\mathcal{O}(mJN)$ elements that differ for a single-dihedral state, and the $J$ diagonal elements. It may be worth noting that this estimate does not take into account any symmetry arguments that might reduce the count. Moreover, it does not consider additional strategies that can be employed to reduce the number of required measures even further. Some consideration about this last point will be discussed in section 5.

We would like to highlight that this is not the only possible choice for the mapping and different strategies might be more or less convenient depending on the system at hand; reference [29] details several possibilities available ranging from the binary mapping (more dense) to the unary encoding (less dense, see references [30, 31] for details). As a general rule, beside the number of qubits needed to store a given amount of information, it is just as important to consider the number of Pauli strings generated by each

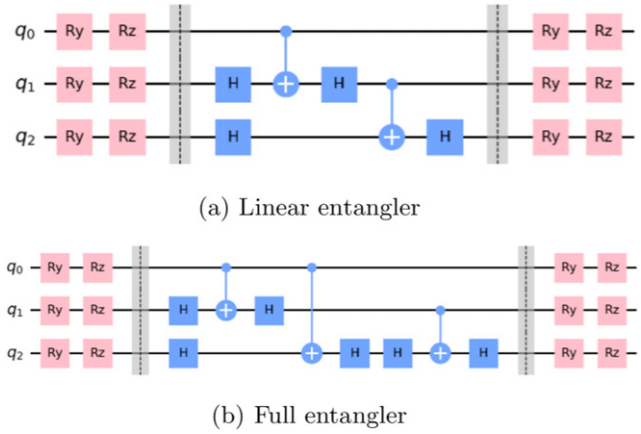


(a) Linear entangler

(b) Full entangler

**Figure 3.** $R_yR_z$ variational forms of depth $d = 1$ with linear (a) or full (b) entangler blocks on a three-qubit circuit.

mapped matrix element and their length (i.e. the number of qubits involved in each string). Generally speaking, a more dense mapping implies longer Pauli strings as more states are encoded in less qubits and viceversa. These different factors must be balanced according to the system and its size.

For the purposes of this paper, the binary mapping is sufficient to give a proof of concept of the applicability of our approach by considering a rather small system. The design of a more efficient mapping is left for future development and discussed in section 5.

### 3.1. Computational details

Here we provide the details about the numerical results shown in section 4. The matrix elements of the FPS operator have been obtained with a homemade C++ code [32] which has also been used as a benchmark for the implementation of the hybrid algorithm with a Python code [33].

In order to evaluate the accuracy and the performance of our method we have considered a chain of three rotors. The resulting two dihedral angles have been parametrized as follows: the first one experiences a bi-stable potential, as dictated by equation (10), while the second one is described by a mono-stable potential as from equation (9). The barrier height $\Delta_r$ for the bistable dihedral has been varied from $0.5k_BT$ to $3.0k_BT$ while the $\Delta_{nr}$ parameter for the single-minimum dihedral has been kept fixed at $1k_BT$. The diffusion coefficients for all three rotors have been set to the same relative value of 1. Due to the structure of equation (11), the term 'relative' refers to the fact that any scaling factor can be applied to the FPS operator to scale the result in terms of the desired diffusion coefficient.

The algorithm has been tested on $Q = 2, 3, 4$ qubit quantum registers using a composite basis set filling completely all the $2^Q$ register states. In order to generate the proper composite basis set for the system an adequate number of single-dihedral basis functions had to be selected according to equations (17) and (18). Indicating the number $n_1$ of isolated basis functions for the double-minimum dihedral and with $n_2$ the ones selected for the single-minimum dihedral, the following $(n_1, n_2)$ basis set have been selected for each value of $Q$: for the two-qubit system a $(4, 2)$ basis set has been employed, for the three-qubit we opted for a $(4, 4)$ configuration and a $(8, 4)$ set has been used for the four-qubit calculations. Note that, due to symmetry restrains, only half of the composite basis functions generated by each $(n_1, n_2)$ set are used in the actual variational procedure.

A $R_yR_z$ heuristic variational circuit has been employed in order to prepare the trial wave-function required in the VQE procedure [34]. Two main elements form such a circuit: a layer of parameterized $R_y$ and $R_z$ rotations, used to apply an arbitrary single qubit rotation to each qubit in the quantum register, and an entangler block to introduce correlation in the trial wave-function. A variational circuit of depth $d = 1$ can be obtained enclosing an entangler block between two rotation layers. Higher depth circuits can be obtained by concatenating couples of entangler blocks and rotation layers to the depth $d = 1$ circuit. A $Q$-qubits $R_yR_z$ circuit of depth $d$ is defined by $2Q(d + 1)$ variational parameters. Two different entangler blocks configurations have been considered in this paper: one creating entanglement between adjacent qubits, hereafter addressed with the name 'linear', and one creating entanglement between all couples of qubits in the register, called 'full' from now on. In figure 3 schematic representations of these parameterized circuits are shown.

As can be seen from such a figure, the entangler block has been implemented using CZ gates instead of pure CNOT gates. This choice ensures an important property: whenever a new qubit, initialized to the $|0\rangle$

state, is added, without additional rotations, to the bottom of a $N$ qubits quantum register, initialized to the state $|\psi_N\rangle$, a product state $|\psi_{N+1}\rangle = |\psi_N\rangle|0\rangle$ is obtained for the overall register. This property will be fundamental for the upcoming discussion and will allow for the application of the hierarchical procedure described in section 4.1.

In order to start the VQE procedure, the register is set to the all-zeros state $|0\rangle$ that has been selected in order to correspond to the basis set function $\phi_0(\theta_1, \theta_2) = \Xi_1(\theta_1)\Xi_0(\theta_2)$ given by the product between the first excited state $\Xi_1(\theta_1)$ of the isolated double-minimum system and the ground-state $\Xi_0(\theta_2)$ of the single-minimum one. This choice is clearly dictated by the physics of the system in which, in absence of coupling, the selected state would represent the exact solution to the kinetic problem. The starting rotation angles of the variational form are set randomly at every run.

Four different optimization algorithm, namely the downhill simplex method, sequential least square programming (SLSQP), constrained optimization by linear approximation (COBYLA) and simultaneous perturbation stochastic approximation (SPSA), have been applied with variable degrees of success based on the type of simulation. The IBM Qiskit module [35] (version 0.22) has been employed for the simulation of the quantum circuits. The implementation has been tested using the built-in Qiskit statevector simulator, an ideal simulator that return the statevector of the quantum register. Then, we characterized the statistics induced by a finite number of measurements of the quantum state in a noiseless quantum simulation varying the number of runs (that are the times a circuit is executed and measured). Finally, the behavior of the algorithm has been tested on a noisy simulator. For this last task, the noise model of the IBMQ Santiago has been employed and a standard readout error mitigation protocol (based on reference [36]) has been applied to each circuit simulation, as implemented in Qiskit.

In order to perform the simulations with the IBMQ Santiago noise model, the built-in Qiskit transpilation routines have been employed to map the circuit on the quantum computer topology. During this process, gates have been translated into $U_1$, $U_2$, $U_3$ and CNOT basis gates. Given the five-qubit inline topology of IBMQ Santiago, the transpilation of a linear entangler $R_yR_z$ variational form on $Q$ qubits appears to be very efficient, resulting in a gate count of $4Q - 3$ ($3Q - 2U_n$ and $Q - 1$ CNOT) without requiring any qubit swap. The transpilation of a full entangler $R_yR_z$ circuit represents instead a more complex task requiring qubit swaps due to the presence of CNOT entagling non-adjacent physical qubits.

The measurement of the expectation value has been carried out either by measuring one-by-one all the Pauli strings of the mapped operator or by relying on Qiskit built-in method which groups together all the terms that are simultaneously diagonalizable [37]. The grouping strategy allowed to reduce the number of Pauli strings to measure independently in all cases (4, 16 and 55 independent circuits to measure 12, 40 and 144 strings respectively for a two, three and four qubits representation of the FPS operator), nevertheless, both methods performed equally well and returned comparable results in presence of a simulated noisy quantum hardware. Finally, we point to reference [38] for an additional useful discussion on the implementation and performances of an efficient computation of expectation values on quantum computers.

## 4. Results

In this section we discuss the results obtained with numerical simulations of the algorithm in several platforms: the Qiskit statevector simulator, the Qiskit quantum assembly simulator (QASM) with and without a noise model and the IBMQ Santiago device [35].

In section 4.1 we assess the variational circuit performance by discussing the results obtained with a noise-free optimization. The importance of this investigation is highlighted by the large amount of research on the ansatz efficiency when this kind of algorithms are applied to quantum chemistry problems [25, 39, 40]. Finally, in section 4.2 we show the results of noisy simulations of the algorithm as a function of the barrier height and number of qubits adopted.

### 4.1. Variational network assessment

The first question we want to address is whether a $R_yR_z$ variational form can produce a good trial wave-function to approximate the classical computational result and if the optimization procedure is able to find its way towards such a configuration.

In order to give a reasonably general picture, a few representative results have been reported in table 1. All the data in table 1 have been obtained from 60 independent VQE optimizations carried out on the Qiskit statevector simulator. For each evaluation the parameters of the $R_yR_z$ variational form have been set randomly and optimized with the SPSA algorithm for a maximum of 600 iterations. The choice of the optimization algorithm has been dictated by a performance analysis carried out on different optimizers

**Table 1.** Results obtained by 60 independent VQE optimizations using the statevector simulations. $Q$ indicates the number of qubits and $\Delta_r$ is the barrier height for the double minimum dihedral. We report $\min(\lambda_1)$ as the minimum value obtained in the simulations, $\langle\lambda_1\rangle$ as the average value, while $\lambda_1^{\text{ref}}$ represents the theoretical target value for the considered basis set obtained with classical calculation. $\varepsilon_{\min}(\%)$ and $\varepsilon_{\text{avg}}(\%)$ are respectively the percentage error on the minimum and on the average.

| $Q$ | $\Delta_r$ | Entangler | $\min(\lambda_1)$ | $\langle\lambda_1\rangle$ | $\lambda_1^{\text{ref}}$ | $\varepsilon_{\min}(\%)$ | $\varepsilon_{\text{avg}}(\%)$ |
|---|---|---|---|---|---|---|---|
| 2 | 0.5 | Linear | 1.516 15 | 1.551 82 | 1.515 62 | 0.0350% | 2.39% |
| 3 | 0.5 | Linear | 1.482 44 | 1.564 13 | 1.475 37 | 0.479% | 6.02 % |
| 3 | 0.5 | Full | 1.491 13 | 1.569 67 | 1.475 37 | 1.07% | 6.39% |
| 4 | 0.5 | Linear | 1.545 94 | 1.819 58 | 1.475 31 | 4.79% | 23.34% |
| 2 | 3.0 | Linear | 0.333 13 | 0.339 94 | 0.333 10 | 0.009 01% | 2.05% |

reported in appendix A. The expectation value has been evaluated at each step with an independent measurement for each of the Pauli strings.

We have chosen to report the minimum value obtained from the sampling as a measure of the heuristic network capability in generating a trial state reasonably close to the optimal configuration; while we have adopted the average converged result to quantify the performance of the optimizer in extracting the desired state from the overall accessible Hilbert space. We are aware that this is a non trivial analysis given that many factors contribute to the shape of the optimization landscape and the exploration of the underlying Hilbert space. Nevertheless, we will see as our considerations are in agreement with more structured studies in literature applied to parametrized quantum circuits [41, 42]. Further, we point to reference [43] where alternative strategies are discussed to quantify the performance of variational ansatz.

As it can be seen from table 1, increasing the number of qubits results in a steep rise of the average value error accompanied by a somewhat milder increase in the error on the minimum value that, even for four qubits, remains under the 5% limit. These data indicate how a $R_yR_z$ variational form of depth $d = 1$ can be used to produce reasonable approximations of the target state with an error, on the expectation value, lower than 1.1% for two and three qubits systems. This finding is in agreement with the general analysis carried out by Sim *et al* [42] where parametrized quantum circuits similar to the ones adopted in this study have shown a good capability of uniformly represent the Hilbert space in which they are defined.

Conversely, the larger error on the distribution average is a clear sign of the challenging optimization process. It is known that such a complexity is not only arising from the dimensionality of the problem, but it is closely related to the phenomenon of quantum tipicality [44, 45], meaning that the distribution of certain functions on the quantum states of a given Hilbert space is extremely peaked around a typical value. Specifically, for random quantum circuits such as the one considered in our case, the average value of the gradient objective function tends to zero and, as the Hilbert dimension increases, more states will correspond to flat regions of the optimization landscape [46, 47].

We also conclude that, because of the small size of the employed quantum registers, there is no advantage in using a full entangler instead of a linear one, as their results are essentially comparable. Despite the full entangler being more expressive than the linear one, the discrepancy observed in the minimum values from table 1 is negligible and probably due to the limited number of VQE runs. Furthermore, in general terms, it is worth noting that a variational ansatz with higher expressibility does not imply having a better convergence: if the ansatz is not very expressive but contains the exact solution of the problem, the optimizer will be able to reach it more easily. A general analysis of the expressibility associated with both the full and linear configurations of the $R_yR_z$ variational forms is presented in appendix B.

In order to clarify how the optimizer convergence impacts the overall VQE outcome, let us observe how a state $|\phi\rangle$ obtained from a $N$-qubit $R_yR_z$ variational form can be exactly reproduced, in the form of $|\phi\rangle \otimes |0\rangle$, with a $(N+1)$-qubit $R_yR_z$ variational ansatz by properly setting the rotation parameters (cf section 3.1). This implies that: given two variational systems, composed respectively by $N$ and $N' > N$ qubits, and considering the proper ordering of the basis-set, the accuracy of the best estimate accessible to the larger $N'$-qubits system must be higher or at least equivalent to the accuracy of the estimate produced by the smaller $N$-qubit one. In order to test this idea, a hierarchical procedure has been devised in which the optimized parameters of a $N$-qubit variational form have been used as the starting guess in a $(N+1)$-qubit VQE procedure. A total of 500 VQE have been carried out using COBYLA optimizer. Differently from what observed in the VQE calculations reported in table 1, a monotonic decrease in the minimum value is encountered in the hierarchical procedure: a minimum value of 1.516 is found for a two-qubit system, a value of 1.484 is encountered for a three-qubit system, while a final value of 1.475 is encountered in the case of four qubits. A similar monotonic decrease is also observed for the distribution averages. We therefore

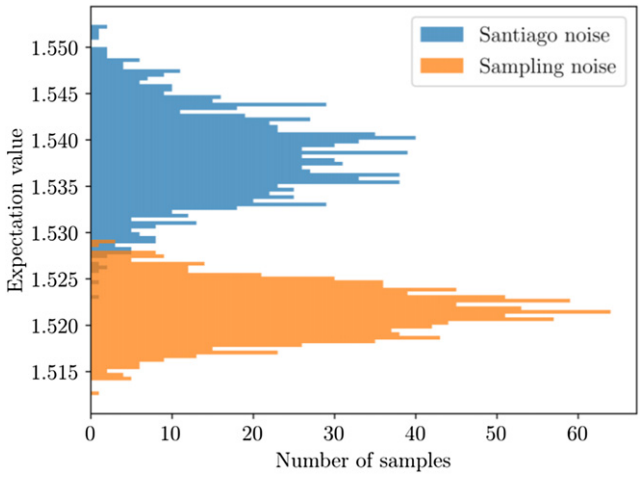


**Figure 4.** Expectation value distribution obtained from 1000 circuit (each one executed 20 000 times) on the same converged $R_yR_z$ parameter set for a two-qubit system with $\Delta_r = 0.5k_BT$ for the bi-stable dihedral. Blue distribution relates to the sampling under the simulated IBMQ Santiago hardware noise; orange distribution is due to finite measurements.

verified that the accuracy of the obtained result increases by enlarging the computational space in the case the optimization procedure is guided by an educated guess.

This observation is fundamental in understanding the nature of the results discussed above, proving that the algorithmic bottleneck for the accuracy is the classical optimization procedure rather than the quantum part. In conclusion, the trends emerging from these calculations are supporting the following considerations: the pure state distribution generated by the two entanglers allows one to reach the configuration corresponding to the global minimum of the optimization landscape but, on the other hand, we have seen that the landscape itself is affected by the dimension of the explorable Hilbert space. This drawback could be overcome by developing physically-inspired ansatz for the Smoluchowski operator similarly to what has been done in the literature for the molecular Hamiltonian [39].

Knowing the limit imposed by an ideal implementation will allow us to independently verify how various types of noise affect the overall stability of the method, as we will see in the following section.

### 4.2. Statistics of finite measurements and quantum noise effects

At this point, we continue our analysis by discussing the effects of different noise sources on the circuits presented above with the aim of answering the question: how does the introduced noise impact the expectation value measurement for a given circuit configuration? This is especially important in the case of nearly-converged configurations in which the error introduced by noise can significantly affect the ability of the optimizer to operate. In order to investigate this point, a converged set of $R_yR_z$ parameters has been used to study the effects of finite measurements and quantum noise on the expectation value. The optimized variational parameters have been obtained using the IBMQ Santiago quantum computer noise-model. To accumulate statistics, we have measured $\langle\hat{\Gamma}\rangle$ with 1000 independent runs. Each Pauli string measurement was accomplished accumulating 20 000 shots. Figure 4 reports the results of this investigation as two distinct distributions for the expectation value in the case of the sole sampling noise or with an addition of a noise model tailored on the IBMQ Santiago device.

Looking at the distributions, one can easily verify how the introduction of a noise model in the simulation causes both an increased distribution amplitude, with the loss of the peaked Gaussian profile observed for the noiseless simulator, and a shift of the average value. This last point is quite interesting since it highlights the profound difference existing between the two effects. The sampling effect stems from an inherent rounding error due to the limited number of measurement performed. As such, for a set of repeated measures it will appear as a Gaussian distribution centered around the exact expectation value for the state prepared by the variational form. Moreover, the variance of the sampling distribution tends to zero as the number of measurements increases. On the other hand, the simulated noise of a NISQ device alters the generation of the trial state producing slightly different wave-functions. Since the trial state, obtained via the optimization procedure, is located near a minimum, most of the error in the state preparation will result in a higher expectation value estimate. The best value obtained in the presence of noise is, indeed, 0.7% higher than the best value obtained in an ideal calculation.

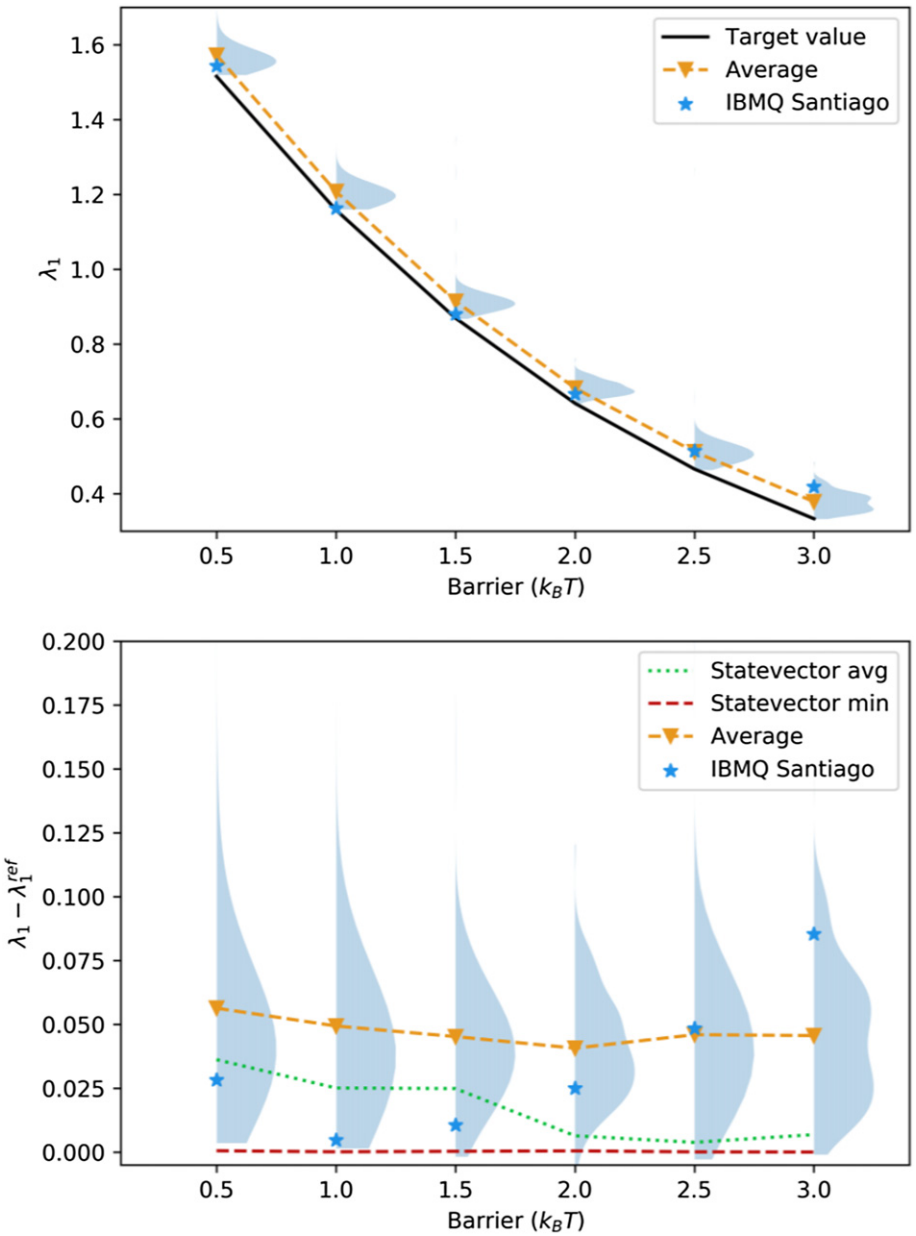


**Figure 5.** (Upper panel)—dependence of the first non-zero eigenvalue $\lambda_1$ with respect to the dihedral barrier height $\Delta_r$. In light blue, we report the distribution obtained from 250 VQE optimizations with random initial guess simulating the circuit execution with a noise model based on the IBMQ Santiago hardware. The black line represents the target value computed for the given basis set while the orange dashed line connects the average value for each group of VQE runs. Blue stars show the results obtained evaluating the last variational circuit (already optimized by the statevector simulator) on the five qubits chip IBMQ Santiago. (Lower panel)—absolute deviation from the target values. Dotted green line shows the average result obtained with a statevector simulation repeated 60 times with different initial guesses.

We now consider how the noise affects the quantum calculation of both different models, by changing the potential energy barrier of the conformational transition, and of different implementations, by changing the number of basis functions describing the target eigenfunction (i.e. using a different number of qubits).

**Performance dependency on the potential barrier height.** For this evaluation we have performed 250 VQE routines starting with a random guess for the $R_yR_z$ parameters. The variational parameters have been optimized using the SPSA algorithm under the effect of the Santiago quantum computer noise model. Every circuit has been transpiled before the simulation. In figure 5, we report the results where two qubits encode the composite dihedral states describing a system of three rotors in which $\Delta_r$ for the double-minimum dihedral has been varied form $0.5k_BT$ to $3.0k_BT$ while $\Delta_{nr}$ for the single-minimum dihedral was kept fixed at $1k_BT$.

First of all, we can notice how, as expected for activated processes, the kinetic constant decreases as we increase the potential energy barrier. Looking at the data, we can observe the good agreement between the

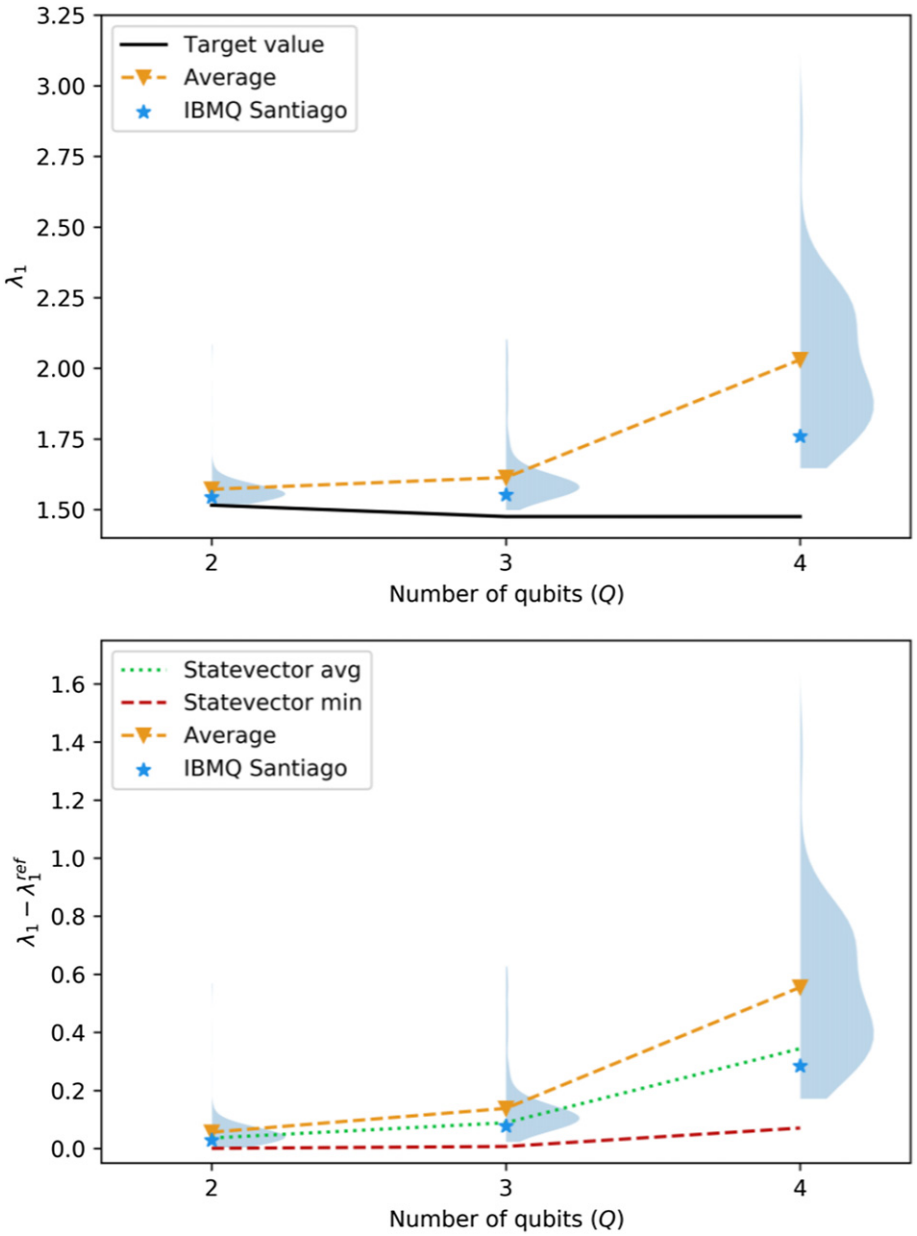


**Figure 6.** (Upper panel)—dependence of the first non-zero eigenvalue $\lambda_1$ with respect to the number of qubits adopted. In light blue we report the distribution obtained from 250 VQE optimizations with random initial guess with a noise model based on the IBMQ Santiago hardware. The black line represents the target value computed for the given basis set while the orange dashed line connects the average value for each group of VQE runs. Blue stars show the results obtained evaluating the last variational circuit (already optimized by the statevector simulator) on the five qubits chip IBMQ Santiago. (Lower panel)—absolute deviation from the target values. Dotted green line shows the average result obtained with a statevector simulation repeated 60 times with different initial guesses.

classically estimated target value (solid line) and the average results obtained with IBMQ Santiago noise model (downward triangles). In the same graph, we report (stars) the values of $\lambda_1$ obtained computing the expectation value on the IBMQ Santiago quantum computer starting from a set of variational parameters optimized using a VQE procedure carried out on the Qiskit statevector simulator. During the expectation value measurement on the IBMQ quantum hardware each circuit has been repeated, in order to build the required statistics, for the maximum allowed number of times (8192 runs). The obtained data, despite being computed from parameters obtained in a completely noiseless procedure, provide a natural metric to look at the results in term of the characteristic noise of a NISQ era quantum computer. These information, together with the ones coming from the noisy simulations, can be seen as a general proof of concept showing the feasibility to run the entire calculation on a NISQ device.

Bearing in mind that the quantum noise affects only the evaluation of the final expectation value, we may notice that adding a further noise source causes sensible deviations from the noise-free average. To comment this results, we leverage the intuition built from the statistical analysis in the previous section: the

points collected on the IBMQ Santiago can be seen as samples of a third distribution generated by the noise of the actual quantum hardware. Under this light, we may notice that in almost all cases we obtain absolute errors comparable with the maximum and mean deviations of the two distributions reported in figure 4.

This result, on the one hand supports the effectiveness of the noise model in capturing the performance of real hardware, and on the other hand allows us to justify the greater deviation from the ideal average at the last point.

Finally, we can also notice that the absolute width of the distribution remains substantially unchanged in the range of barriers explored. As a consequence, the relative error decreases moving from higher to smaller barriers passing from 13.6% at $3.0k_BT$ to 3.72% at $0.5k_BT$. In the same figure (lower panel), the noise-free statevector results are reported as reference. Here, we can appreciate with more the detail that, even though the distribution width is almost constant, the optimization is more sensitive with respect to the initial guess distribution for small barrier values.

**Performance dependency on the basis set size.** Now that the accuracy of the algorithm has been discussed in terms of the physics of the simulated system, a final question still remains open: how does the performance of the protocol scales with the number of qubits employed? To answer to such a question, we consider the same system of a three rotor chain with reactive barrier height of $\Delta_r = 0.5k_BT$. The probability density distribution has been described adopting an increasing number of basis elements from 4 up to 16 odd composite functions (see equation (17)). This translates to an increasing number of qubits to encode the overall probability density distribution. The purpose of this analysis is not to assess the accuracy of the basis set size (which determines only a slight change in the kinetic rate constant), but to observe the effect of a noisy device upon performing the same calculation with an increasing number of quantum resources. The results obtained in such a simulation, together with the reference values, are reported in figure 6.

As we can see, the distribution width rapidly increases with the number of qubits and so does also the average expectation value computed with both statevector and noisy simulators. This points out the increased complexity of the optimization procedure as previously mentioned in section 4.1. For a four qubits system, an error of the 37.6% is recovered for the noisy simulation, while an error of the 23.3% is encountered in the case of a statevector simulation. These data confirm the role of the noise in creating less accurate predictions, but also shows how a significant part of the error itself should be ascribed to a difficult convergence of the classical optimization as anticipated in section 4.1. This massive performance degradation has also the effect of hiding the tiny margin for accuracy improvement induced by the basis-set extension. This is a critical aspect to consider in this early VQE implementations in which a good trade-off between algorithm stability and basis-set extension must be found. Further analyses of possible alternative variational networks could circumvent this issue.

## 5. Conclusions

In this paper, we have presented a novel application for quantum computers. Particularly, we have addressed the solution of the Fokker–Planck–Smoluchowski eigenvalue problem exploiting its isomorphism with the Schrödinger equation.

The proposed algorithm consists of three main ingredients: (i) a strategy to map the classical probability distribution onto the quantum register, (ii) the choice of a unitary ansatz to generate trial probability distributions (in the same spirit of the original VQEs for quantum systems) and (iii) the implementation of a classical optimization routine updating the unitary control parameters to move towards the exact configuration. Further investigation should follow along all the lines mentioned above.

Indeed, in order to devise a quantum algorithm useful for everyday applications and able to achieve quantum advantage with respect to a classical solution, a polynomial scaling of the quantum resources with the system size is desirable. Our analysis in section 3 has shown how this has already partially been achieved considering the information storage point of view. On the other hand, a dense mapping such as the binary approach adopted insofar requires a number of measurements that scales exponentially with the number of rotors in the chain. This aspect can be mitigated by implementing different strategies that group sets of Pauli strings reducing the overall measurement count [37, 48–50]. In this regard it is important to notice that the goal of these strategies is to find groups of Pauli strings that commute as, in that case, it is possible to find a joint eigenbasis of the quantum computer state in which they are measurable. This is a non-trivial task and in general it is not easy to estimate the gain compared to a serial evaluation of all the Pauli strings. As a simple instance of these methodologies, we can think of the $J$ diagonal elements of the FPS operator for which a single circuit execution is sufficient since all the strings are diagonal in the computational basis and can be measured simultaneously. Despite this, looking at systems of interest from an application point of view a step forward is still needed.

In a future work, we will seek to overcome this issue by developing a mapping on the single-dihedral states which should reduce dramatically the number of terms in the FPS operator representation. In quantum chemistry parlance, this would correspond to a mapping on the spin-orbitals in place of a mapping on the Slater determinant basis.

Other matters to be addressed concern the unitary ansatz generating the trial probability distribution and the classical optimizer. These aspects have been considered in section 4. There, we have shown that adopting a $R_yR_z$ heuristic variational network allows to achieve good results for a small basis set. We believe that the results we have obtained in presence of a simulated noise can be further improved by the incorporation of a mitigation routine such as the zero noise error extrapolation [51]. However, we decided to not include also this feature in the implementation as it goes beyond the purpose of the present study of presenting a new application of hybrid algorithms in the field of stochastic processes.

At the same time, we have also noticed that the performance scales poorly with respect to the number of qubits and suffers of some problems deriving from the uniform and agnostic coverage of the underlying Hilbert space. In this direction we have suggested as a working strategy to lower the barrier of the optimization task by applying an hierarchical procedure in which the solution of the variational optimization with a smaller number of basis function is used as initial guess for the estimation of the kinetic rate constant using an higher number of qubits. Such an approach is in line with the development of algorithms in the NISQ era where small quantum processors are put to test by very shallow circuits; alternatively, we should look at further refinements of this implementation by developing physically-inspired ansatz as done in other contexts. Also this aspect will be investigated in a future work.

In essence, we achieved the proof of concept of the application of a quantum computer to solve stochastic dynamics. With some technical developments as discussed in the previous paragraphs, the proposed procedure brings stochastic dynamics amongst the promising applications of future quantum devices.

## Acknowledgments

We are grateful to Prof. Ivano Tavernelli for fruitful discussions. We acknowledge the use of IBM Quantum services for this work. The views expressed are those of the authors, and do not reflect the official policy or position of IBM or the IBM Quantum team. We acknowledge the support by the DOR funding schemes of the Dipartimento di Scienze Chimiche, Università di Padova. PP is grateful to Fondazione CARIPARO for financial support (PhD Grant). PP is grateful to the Cloud Veneto computing infrastructure for the computation time granted under the project 'Nuclear quantum effects'. DC is grateful to MIUR 'Dipartimenti di Eccellenza' under the project Nanochemistry for energy and Health (NExuS) for funding the PhD Grant.

## Data availability statement

The data that support the findings of this study are available upon reasonable request from the authors.

## Appendix A

In what follows the optimizer selection and the effect that the entangler type has on the convergence behavior of the algorithm will be presented. Addressing the discussion of this problem is not trivial since the convergence profile of each VQE routine depends upon the selected set of initial parameters. We will proceed by analyzing, for different choices of optimizer and entangler, the convergence profile of a single VQE. This clearly represents only a single point in the multidimensional initial parameter space and consequently only comparative considerations can be done between different methods. Such a simple data representation, visible in figure 7, can anyway already give a useful qualitative picture. For the present tests, a three qubit system is considered; both dihedral barriers (single and double) have been set to $1k_BT$ and a common set of randomly selected initial parameters has been kept fixed for all simulations. The built-in Qiskit SPSA optimizer together with the Nelder–Mead, SLSQP and COBYLA optimizer from the SciPy [52] Python module have been employed. The figure contains three plots that represent the profile of the VQE optimization in the case of various type of noise. The top panel contains data obtained using the (noiseless) statevector simulator. The center panel represents a noiseless simulator in which the number of measures on the same circuit has been set to 20 000. The lower panel shows the results for the transpiled circuits simulated including the noise model of the IBMQ Santiago quantum computer. Also for this last case the number of runs has been set to 20 000.

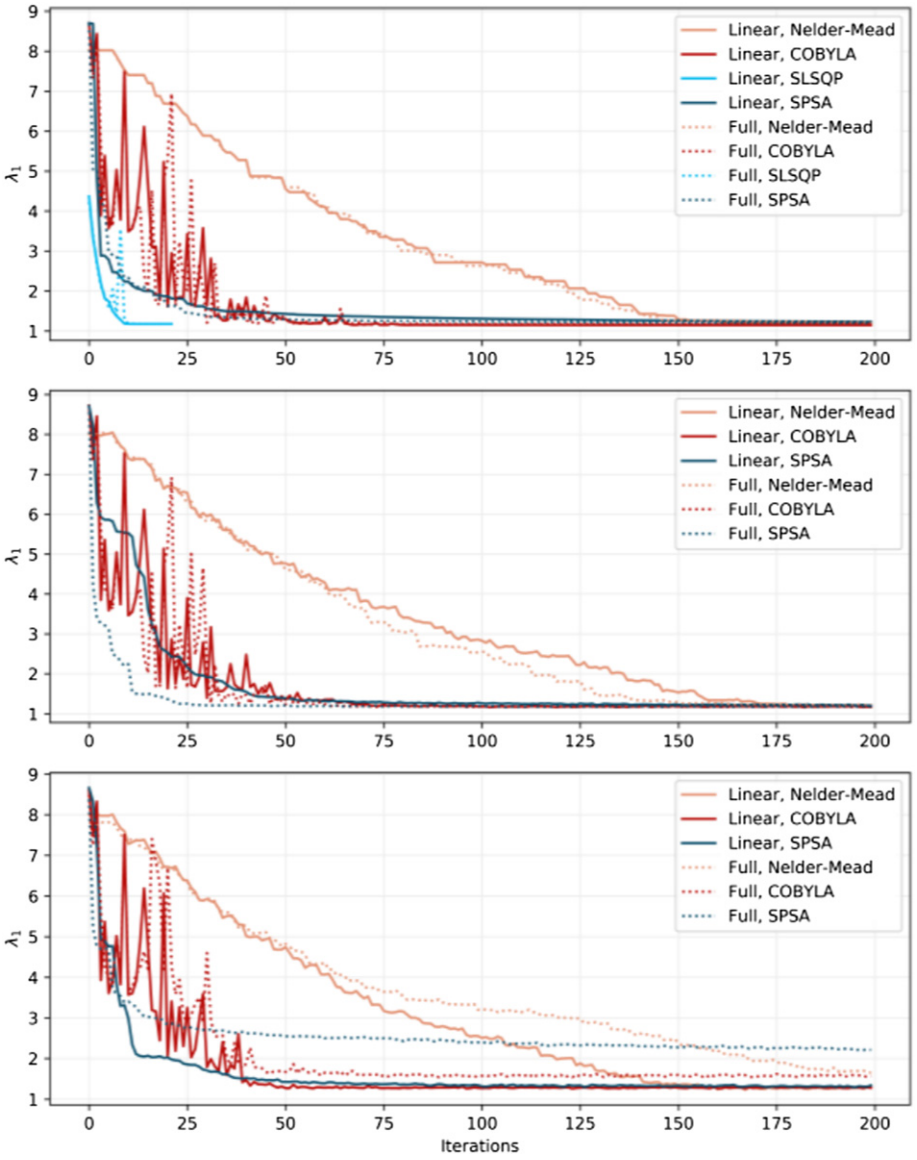


**Figure 7.** Comparison between single VQE optimization under different conditions of optimizer and entangler. The tree graphs refers to the results obtained with the Qiskit statevector simulator (higher panel), Qiskit QASM without (central panel) and with (lower panel) the IBMQ Santiago noise model. For the middle and lower panel the number of measures on the same circuit has been set to 20 000.

Analyzing figure 7 many interesting comments can be made. First of all looking at the raw performance of the various optimizers one can easily observe how the Nelder–Mead algorithm consistently shows a slower convergence toward the target value if compared with the other optimization procedures. The SLSQP algorithm shows very good performance in the statevector simulations converging in few iterations to the target value; however its sensitivity to noise prevent, as far as we can tell, its application to noisy simulations. Both COBYLA and SPSA shows consistently stable and reasonably good performances with the latter showing a more consistent behaviour and greater accuracy in simulations with higher noise. For this reason SPSA has been used as the default optimizer throughout the paper. Looking at the central panel one can easily see how little difference is observed between different entanglers in term of converged values with the full entangler resulting mildly more accurate. As it can be seen in the lower panel, the situation is rapidly reversed by the introduction of a realistic quantum computer noise model. The more complex structure of the full entangler joined with the less efficient transpilation, results in a slower converging and significantly less accurate result, clearly pointing to the linear entangler as the natural candidate for a realistic implementation.

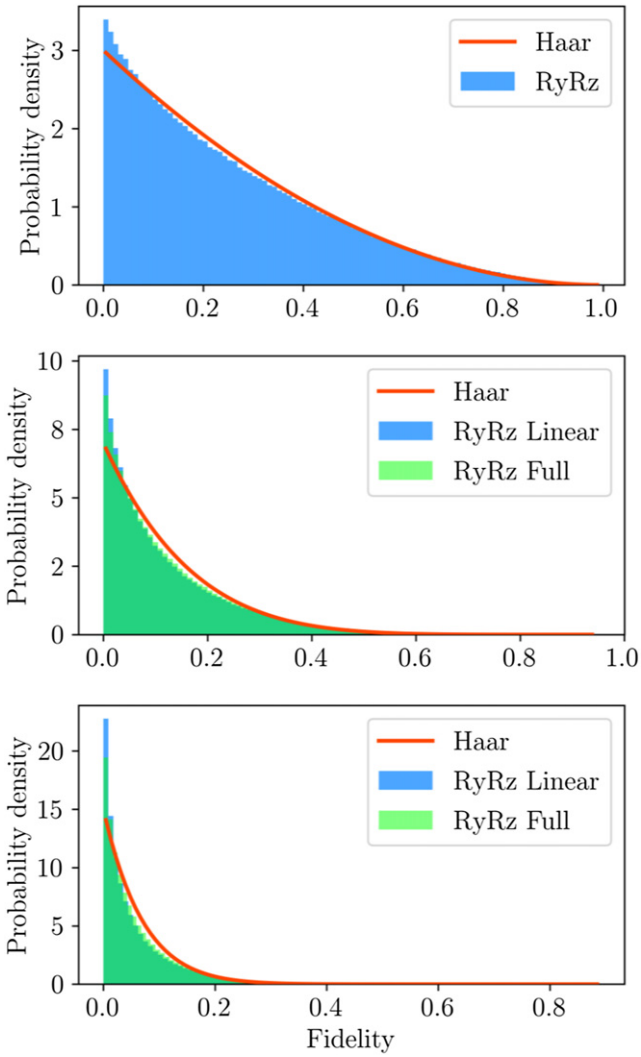


**Figure 8.** Each panel reports the fidelity distribution obtained from couples of states generated from a random choice of the $R_yR_z$ variational parameters (blue: linear entangler, green: full entangler) and the fidelity distribution expected for a set of Haar-random states (red line). The variational form depth has been set to 1. From the top to the bottom the case of two, three and four qubits are reported.

**Table A1.** Expressibility values associated to different configurations of an $R_yR_z$ variational form of depth 1 for a variable number of qubits $Q$.

| $Q$ | Linear | Full |
|---|---|---|
| 2 | $1.93 \times 10^{-3}$ | — |
| 3 | $2.01 \times 10^{-2}$ | $9.03 \times 10^{-3}$ |
| 4 | $5.78 \times 10^{-2}$ | $2.27 \times 10^{-2}$ |

## Appendix B

In what follows the expressibility, i.e. the ability of a quantum circuit to generate pure state that are well representative of the Hilbert space, will be evaluated for the case of the $R_yR_z$ variational form adopted in this paper. To do so, the procedure described by Sim *et al* [42] has been applied for the case of two, three and four qubits configurations.

Firstly, we have computed the fidelity of $1 \times 10^6$ pairs of random states obtained by sampling random parameters for the variational ansatz. The obtained distributions of both the linear and full entanglers are shown in figure 8. We also report the fidelity distribution of the ensemble of Haar random states (red line), obtained analytically [53], that represents the uniform distribution of states over the Hilbert space. Finally, the expressibility values reported in table A1 have been calculated by taking the Kullback–Leibner

divergence between the fidelity distributions of the ansatz and that of the Haar ensemble. The lower the divergence (i.e. the lower the value of the expressibility), the better the uniform coverage of the Hilbert space. For more details we refer to the original paper [42] and to the recent reference [54] that we found clarifying.

As can be seen from the results, the $R_yR_z$ variational form considered in this work ensures a good coverage of the Hilbert space. As expected, the full entangler appears to be slightly more expressive (lower expressibility value) than the linear one that, nevertheless, still conserves a reasonably uniform state-space coverage. This supports our claim that the expressibility of our circuits should play a modest role in algorithmic convergence, which is mainly dominated by the behavior of the optimizer.

## ORCID iDs

Pierpaolo Pravatto https://orcid.org/0000-0002-4281-4147
Davide Castaldo https://orcid.org/0000-0001-8622-175X
Federico Gallina https://orcid.org/0000-0002-3694-6397
Barbara Fresch https://orcid.org/0000-0002-0988-0644
Stefano Corni https://orcid.org/0000-0001-6707-108X
Giorgio J Moro https://orcid.org/0000-0003-3905-3831

## References

[1] Deutsch I H 2020 Harnessing the power of the second quantum revolution *PRX Quantum* **1** 020101
[2] Terhal B M 2018 Quantum supremacy, here we come *Nat. Phys.* **14** 530–1
[3] Georgescu I M, Ashhab S and Nori F 2014 Quantum simulation *Rev. Mod. Phys.* **86** 153
[4] McClean J R, Romero J, Babbush R and Aspuru-Guzik A 2016 The theory of variational hybrid quantum–classical algorithms *New J. Phys.* **18** 023023
[5] Jurcevic P *et al* 2021 Demonstration of quantum volume 64 on a superconducting quantum computing system *Quantum Sci. Technol.* **6** 025020
[6] McArdle S *et al* 2020 Quantum computational chemistry *Rev. Mod. Phys.* **92** 015003
[7] Kandala A *et al* 2017 Hardware-efficient variational quantum eigensolver for small molecules and quantum magnets *Nature* **549** 242–6
[8] Ollitrault P J, Baiardi A, Reiher M and Tavernelli I 2020 Hardware efficient quantum algorithms for vibrational structure calculations *Chem. Sci.* **11** 6842–55
[9] Yoshioka N and Mizukami W 2020 Variational quantum simulation for periodic materials (arXiv:2008.09492)
[10] Nachman B *et al* 2021 Quantum algorithm for high energy physics simulations *Phys. Rev. Lett.* **126** 062001
[11] Haven E E 2002 A discussion on embedding the Black–Scholes option pricing model in a quantum physics setting *Physica*A **304** 507–24
[12] Lin Y, Jiang D and Xia P 2014 Long-time behavior of a stochastic SIR model *Appl. Math. Comput.* **236** 1–9
[13] Singh S K, Thantanapally C and Ansumali S 2016 Gaseous microflow modeling using the Fokker–Planck equation *Phys. Rev.* E **94** 063307
[14] Miyazawa T 1989 Theory of the one-variable Fokker–Planck equation *Phys. Rev.* A **39** 1447
[15] Elber R, Makarov D E and Orland H 2020 *Molecular Kinetics in Condensed Phases: Theory, Simulation, and Analysis* (New York: Wiley)
[16] Helfand E 1978 Brownian dynamics study of transitions in a polymer chain of bistable oscillators *J. Chem. Phys.* **69** 1010–8
[17] Moro G J 1991 The coupling between librational motions and conformational transitions in chain molecules. A phenomenological analysis *J. Chem. Phys.* **94** 8577–91
[18] Moro G J 1992 The coupling between librational motions and conformational transitions in chain molecules: II. The rotor chain represented by the master equation for site distributions *J. Chem. Phys.* **97** 5749–65
[19] Doi M and Edwards S F 1988 *The Theory of Polymer Dynamics* vol 73 (Oxford: Oxford University Press)
[20] Kramers H A 1940 Brownian motion in a field of force and the diffusion model of chemical reactions *Physica* **7** 284–304
[21] Hänggi P, Talkner P and Borkovec M 1990 Reaction-rate theory: fifty years after Kramers *Rev. Mod. Phys.* **62** 251
[22] Van Kampen N G 1992 *Stochastic Processes in Physics and Chemistry* (Amsterdam: North-Holland)
[23] Gardiner C W *et al* 1985 *Handbook of Stochastic Methods* vol 3 (Berlin: Springer)
[24] Jüngel A 2016 Fokker–Planck equations *Entropy Methods for Diffusive Partial Differential Equations* (Berlin: Springer) pp 19–44
[25] Peruzzo A *et al* 2014 A variational eigenvalue solver on a photonic quantum processor *Nat. Commun.* **5** 1–7
[26] Colless J I *et al* 2018 Computation of molecular spectra on a quantum processor with an error-resilient algorithm *Phys. Rev.* X **8** 011021
[27] Ollitrault P J *et al* 2020 Quantum equation of motion for computing molecular excitation energies on a noisy quantum processor *Phys. Rev. Res.* **2** 043140
[28] Higgott O, Wang D and Brierley S 2019 Variational quantum computation of excited states *Quantum* **3** 156
[29] Sawaya N P D *et al* 2020 Resource-efficient digital quantum simulation of d-level systems for photonic, vibrational, and spin-s Hamiltonians *npj Quantum Information* **6** 1–13
[30] McArdle S, Mayorov A, Shan X, Benjamin S and Yuan X 2019 Digital quantum simulation of molecular vibrations *Chem. Sci.* **10** 5725–35
[31] Castaldo D, Rosa M and Corni S 2021 Quantum optimal control with quantum computers: a hybrid algorithm featuring machine learning optimization *Phys. Rev.* A **103** 022613
[32] Pravatto P *et al* 2021 Smoluchowski-Rotor-Chain *GitHub* https://github.com/ppravatto/Smoluchowski-Rotor-Chain/releases/tag/v0.1.0

[33] Pravatto P et al 2021 Binary-VQE GitHub
[34] Moll N et al 2018 Quantum optimization using variational algorithms on near-term quantum devices Quantum Sci. Technol. 3 030503
[35] Aleksandrowicz G et al 2019 Qiskit: an open-source framework for quantum computing (https://zenodo.org/record/2562111)
[36] Fiurášek J 2001 Maximum-likelihood estimation of quantum measurement Phys. Rev. A 64 024102
[37] Bravyi S et al 2017 Tapering off qubits to simulate fermionic Hamiltonians (arXiv:1701.08213)
[38] Verteletskyi V, Yen T-C and Izmaylov A F 2020 Measurement optimization in the variational quantum eigensolver using a minimum clique cover J. Chem. Phys. 152 124114
[39] Wecker D, Hastings M B and Troyer M 2015 Progress towards practical quantum variational algorithms Phys. Rev. A 92 042303
[40] Babbush R et al 2018 Low-depth quantum simulation of materials Phys. Rev. X 8 011044
[41] Woitzik A J C et al 2020 Entanglement production and convergence properties of the variational quantum eigensolver Phys. Rev. A 102 042402
[42] Sim S, Johnson P D and Aspuru-Guzik A 2019 Expressibility and entangling capability of parameterized quantum circuits for hybrid quantum-classical algorithms Adv. Quantum Technol. 2 1900070
[43] Consiglio M et al 2021 Variational quantum eigensolver for SU ($N$) fermions (arXiv:2106.15552)
[44] Popescu S, Short A J and Winter A 2006 Entanglement and the foundations of statistical mechanics Nat. Phys. 2 754–8
[45] Fresch B and Moro G J 2013 Typical response of quantum pure states Eur. Phys. J. B 86 1–13
[46] McClean J R et al 2018 Barren plateaus in quantum neural network training landscapes Nat. Commun. 9 1–6
[47] Cerezo M et al 2021 Cost function dependent barren plateaus in shallow parametrized quantum circuits Nat. Commun. 12 1–12
[48] Hamamura I and Imamichi T 2020 Efficient evaluation of quantum observables using entangled measurements npj Quantum Information 6 1–8
[49] Huggins W J et al 2021 Efficient and noise resilient measurements for quantum chemistry on near-term quantum computers npj Quantum Information 7 1–9
[50] Izmaylov A F, Yen T-C, Lang R A and Verteletskyi V 2019 Unitary partitioning approach to the measurement problem in the variational quantum eigensolver method J. Chem. Theory Comput. 16 190–5
[51] Giurgica-Tiron T et al 2020 Digital zero noise extrapolation for quantum error mitigation 2020 IEEE Int. Conf. on Quantum Computing and Engineering (QCE) (Piscataway, NJ: IEEE) pp 306–16
[52] Virtanen P et al 2020 SciPy 1.0: fundamental algorithms for scientific computing in Python Nat. Methods 17 261–72
[53] Życzkowski K and Sommers H-J 2005 Average fidelity between random quantum states Phys. Rev. A 71 032313
[54] Hubregtsen T, Pichlmeier J, Stecher P and Bertels K 2021 Evaluation of parameterized quantum circuits: on the relation between classification accuracy, expressibility, and entangling capability Quantum Machine Intelligence 3 9